Microtubule dynamics at low temperature: evidence that tubulin recycling limits assembly

Gabriella Li and Jeffrey K. Moore*
Department of Cell and Developmental Biology, University of Colorado School of Medicine, Aurora, CO 80045

ABSTRACT How temperature specifically affects microtubule dynamics and how these lead to changes in microtubule networks in cells have not been established. We investigated these questions in budding yeast, an organism found in diverse environments and therefore predicted to exhibit dynamic microtubules across a broad temperature range. We measured the dynamics of GFP-labeled microtubules in living cells and found that lowering temperature from 37°C to 10°C decreased the rates of both polymerization and depolymerization, decreased the amount of polymer assembled before catastrophes, and decreased the frequency of microtubule emergence from nucleation sites. Lowering to 4°C caused rapid loss of almost all microtubule polymer. We provide evidence that these effects on microtubule dynamics may be explained in part by changes in the cofactor-dependent conformational dynamics of tubulin proteins. Ablation of tubulin-binding cofactors (TBCs) further sensitizes cells and their microtubules to low temperatures, and we highlight a specific role for TBCB/Alf1 in microtubule maintenance at low temperatures. Finally, we show that inhibiting the maturation cycle of tubulin by using a point mutant in β-tubulin confers hyperstable microtubules at low temperatures and rescues the requirement for TBCB/Alf1 in maintaining microtubule polymer at low temperatures. Together, these results reveal an unappreciated step in the tubulin cycle.

INTRODUCTION

Microtubules are distinct from other cytoskeletal polymers in that they rapidly alternate between phases of polymerization and depolymerization, a nonequilibrium behavior known as "dynamic instability" (Mitchison and Kirschner, 1984). This behavior depends on a cycle of nucleotide-dependent conformational changes in the heterodimeric αβ-tubulin subunits that form microtubules (Hyman *et al.*, 1995; Alushin *et al.*, 2014; Geyer *et al.*, 2015). Each heterodimer binds two molecules of GTP (Weisenberg *et al.*, 1968; Berry and Shelanski, 1972). One GTP is sandwiched between α and β and is neither exchanged nor hydrolyzed (Spiegelman *et al.*, 1977). The other GTP binds to an exposed site on β, known as the exchangeable site or "E-site." This nucleotide exchanges rapidly in solution and is hydrolyzed to GDP during microtubule polymerization (Carlier and Pantaloni, 1981; Correia and Williams, 1983; Purich and Kristofferson, 1984). The binding of GTP to the E-site promotes tubulin polymerization and microtubule nucleation, so these rates exhibit a proportional dependence on the concentration of available GTP (Carlier *et al.*, 1987). Polymerization and nucleation rate also strongly depend on the concentration of tubulin (Olmsted *et al.*, 1974; Walker *et al.*, 1988). In the microtubule polymer, tubulin hydrolyzes the E-site GTP and undergoes conformational changes that weaken binding to neighboring tubulins (Carlier and Pantaloni, 1981; Hyman *et al.*, 1995; Alushin *et al.*, 2014). These conformational changes have been described in great detail by recent cryo-EM studies, and the process is referred to as "maturation" (Alushin *et al.*, 2014; Zhang *et al.*, 2015; Manka and Moores, 2018). When microtubules switch from polymerization to depolymerization, an event known as catastrophe, mature GDP-bound tubulin is released from the lattice. GDP-bound tubulin dimers exhibit an approximately sixfold higher dissociation constant than GTP-bound tubulin, but can still contribute to microtubule assembly under in vitro conditions with sufficient

concentrations of tubulin and Mg^{2+} (Carlier and Pantaloni, 1978; Hamel *et al.*, 1986). Together, this evidence indicates that tubulin cycles between different states. The "assembly-competent" state is characterized by GTP binding at the E-site and an extended conformation of the heterodimer that favors interactions with other tubulins. In contrast, the product of microtubule disassembly is presumed to be tubulin in the "assembly-incompetent" state, which features GDP bound to the E-site and a compacted conformation of the heterodimer that disfavors interactions with other tubulins.

Although the assembly activity of tubulin and its relation to nucleotide status is well established, one important, but unanswered, question is how tubulin that has disassembled from a microtubule transitions from the assembly-incompetent state back to an assembly-competent state. Previous studies have shown that cold temperatures can promote the formation of tubulin oligomers as a product of disassembly in vitro. As protofilaments peel away in a "ram's horn" shape, oligomers of curved tubulin are released from the microtubule (Bordas *et al.*, 1983; Lange *et al.*, 1988; Mandelkow *et al.*, 1991). Increasing temperature causes these oligomers to dissociate into heterodimers (Bordas *et al.*, 1983). Despite this evidence of temperature-dependent tubulin oligomers from in vitro experiments, what remains unknown is whether these structures occur in vivo and whether they represent points for regulating the pool of assembly-competent tubulin.

A potential mechanism for regulating the pool of assembly-competent tubulin would be to co-opt the tubulin biogenesis pathway. Tubulin biogenesis requires prefoldin and cytosolic chaperonin containing TCP-1 (CCT) to begin folding nascent α- and β-tubulin after translation (Yaffe *et al.*, 1992; Tian *et al.*, 1996; Vainberg *et al.*, 1998). However, unlike actin and other proteins that require CCT activity, tubulin also requires an additional set of tubulin-binding cofactors (TBCs) which bring together α- and β-tubulin subunits to form the assembly-competent heterodimer (Gao *et al.*, 1993; Tian *et al.*, 1997). In addition to their roles in tubulin biogenesis, TBCs also appear to regulate the activity of preformed heterodimers. In vitro, TBCC, TBCD, and TBCE form a complex that binds to preformed heterodimers and acts as a GTPase-activating protein (GAP) for tubulin in the absence of microtubule polymerization (Tian *et al.*, 1999; Nithianantham *et al.*, 2015). Both TBCC and TBCE have each been shown to disassemble heterodimers in vitro, and overexpression of either in HeLa cells leads to microtubule loss (Bhamidipati *et al.*, 2000). The dissociation of tubulin heterodimers by TBCE is enhanced greatly by the presence of TBCB, together forming a tripartite complex of TBCE, TBCB, and α-tubulin (Kortazar *et al.*, 2007; Serna *et al.*, 2015). These results demonstrate that TBCs can act on already formed tubulin heterodimers to alter nucleotide-binding status and interactions between tubulins. While it is unclear whether TBCs play a role in the transition of assembly-incompetent, GDP-bound tubulin back to an assembly-competent, GTP-bound heterodimer, it has been proposed that TBCs could provide a quality control mechanism to regulate the concentration of GTP-bound tubulin in cells (Tian and Cowan, 2013).

The exquisite temperature sensitivity of microtubule dynamics provides a potential window for gaining insight into these questions. Early studies of cytoskeletal polymers found that microtubules are uniquely cold sensitive and quickly disappear on incubation at low temperatures (Tilney and Porter, 1967; Weisenberg, 1972; Weber *et al.*, 1975; Breton and Brown, 1998). In fact, this property of tubulin is routinely used in protocols for purifying tubulin through cycles of temperature-induced polymerization and depolymerization (Olmsted and Borisy, 1973; Borisy *et al.*, 1975). The cold sensitivity of tubulin stands in contrast to F-actin polymers which persist after exposure to low temperatures (Breton and Brown, 1998). The loss of microtubule polymer at low temperatures suggests a unique disruption of the normal tubulin cycle that may trap tubulin in an assembly-incompetent state.

In this study, we sought to determine how low temperature impacts the tubulin cycle to lead to the loss of microtubules in vivo. We used the budding yeast model, which has several major advantages for our study. Budding yeast have a simple microtubule network allowing for the measurement of single astral microtubules while possessing only one β-tubulin and two α-tubulin isotypes, thus forming a more homogeneous tubulin pool than that found in higher eukaryotes. Furthermore, yeasts are found in diverse environments around the world, including budding yeasts that live in terrestrial environments with low temperatures and yeasts that live in marine environments (Libkind *et al.*, 2011; Gladfelter *et al.*, 2019). This suggests that yeast tubulin may exhibit a broader dynamic range of temperature response. We find that the rates of yeast microtubule polymerization and depolymerization are proportional to temperature and provide evidence that TBCs promote tubulin activity at low temperatures. We propose a model in which low temperatures trap tubulin in an assembly-incompetent state, and the pathway involved in tubulin biogenesis may help return it to assembly competence.

RESULTS

Temperature dependence of microtubule dynamics in vivo

While the cold sensitivity of microtubules has been known for years, how temperature affects the properties of microtubule dynamics remains poorly understood. We began by testing the hypothesis that microtubules fail to assemble at low temperatures because the rate of microtubule polymerization may be more temperature dependent than the rate of depolymerization. This hypothesis predicts that the polymerization rate will decrease more sharply as temperature decreases compared with the depolymerization rate. To test this prediction, we measured the lengths of single GFP–Tub1-labeled astral microtubules over time in cells incubated at different temperatures (Figure 1, A and B). We controlled temperature using a stage-top microfluidic device, shifting from our standard temperature (30°C) to the target temperature for ~10 min before imaging (see *Materials and Methods*). In our experimental setup, 10°C was the lowest temperature that could be stably maintained during imaging. At the other end of our temperature range, we found similar phenotypes for 37°C and 39°C; but temperatures higher than 39°C severely inhibited microtubule assembly (unpublished data). Within the range from 37°C to 10°C, we find that median astral microtubule length observed per cell over 10 min tended to decrease when the temperature was lowered (Figure 1C).

We used the full data set of microtubule length measurements over time to calculate different parameters of individual astral microtubule dynamics. As expected, polymerization rates of astral microtubules decrease as temperature decreases from 37°C to 10°C (Figure 1D; Table 1). We also found that depolymerization rates decrease across this temperature range (Figure 1E; Table 1). The Arrhenius plot in Figure 1F depicts the rates of change for polymerization and depolymerization across temperatures. As temperature decreases, the rate of depolymerization slows faster than the rate of polymerization, and these rates are predicted to intersect at ~13°C (Figure 1F). Based on these results, the decrease in microtubule polymerization rate at low temperatures (<13°C) would be expected to be offset by slower depolymerization. Therefore, the loss of microtubule polymer at low temperatures cannot be explained by changes in polymerization and depolymerization rates alone.
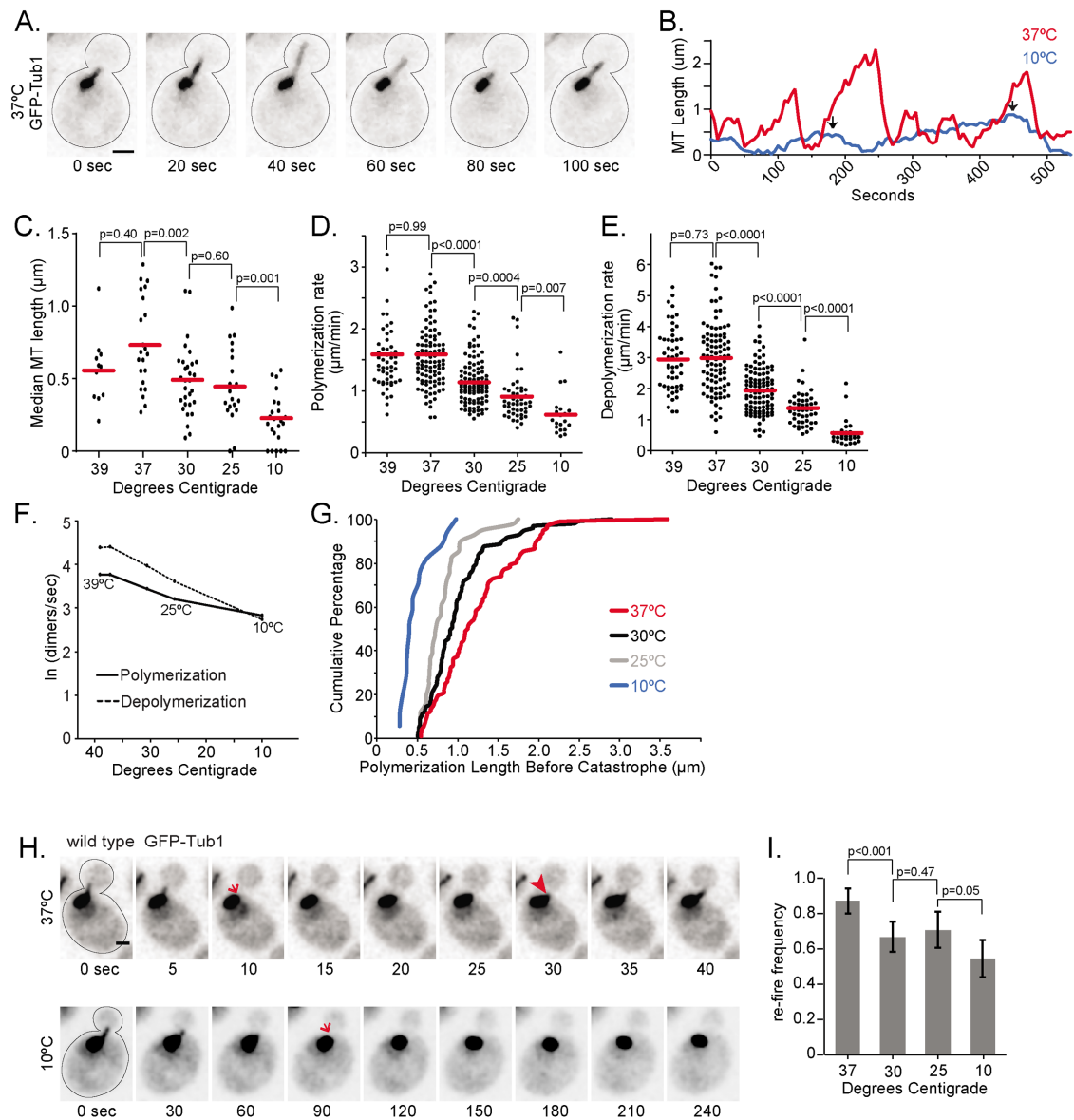
FIGURE 1: Temperature dependence of microtubule dynamics in vivo. (A) Time-lapse image series of a wild-type cell expressing GFP-Tub1, showing the dynamics of a single astral microtubule at 37°C. Scale bar, 1 μm. (B) Lifeplots of single astral microtubules at 10°C (blue) and 37°C (red). Microtubule lengths were measured at 5-s intervals. Arrows indicate measured catastrophe events at 10°C. (C) Median astral microtubule lengths from time-lapse imaging at indicated temperatures. Each dot represents the median length from one cell imaged for 10 min. For C–E, data were collected from at least three separate experiments; $n = 23$ cells at 10°C, $n = 21$ cells at 25°C, $n = 30$ cells at 30°C, $n = 22$ cells at 37°C, and $n = 11$ cells at 39°C. Line indicates mean. (D) Polymerization rates of astral microtubules at indicated temperatures. Each dot represents a polymerization event. Line indicates mean. (E) Depolymerization rates of astral microtubules at indicated temperatures. Each dot represents a depolymerization event. Line indicates mean. (F) Arrhenius plot depicting the natural log of polymerization (solid line) and depolymerization (dashed line) rates extrapolated to dimers per second as a function of the inverse temperature in Kelvin. (G) Cumulative percentage of microtubule lengths at catastrophe at 10°C (blue), 25°C (gray), 30°C (black), and 37°C (red). (H) Image series of wild-type cells with single dynamic astral microtubules labeled with GFP-Tub1 at 37°C (top) and 10°C (bottom). Arrows indicate when microtubule lengths drop below 0.213 μm. Arrowhead indicates when a microtubule "refires" in the cell at 37°C, and the length increases beyond 0.213 μm. Scale bar, 1 μm. (I) Refire frequencies calculated from cells imaged for 10 min at indicated temperatures. Values represent the sum of microtubules that refire within 20 s divided by the sum of microtubules that depolymerize to lengths less than 0.213 μm from at least 20 cells at each temperature. Error bars are standard error of proportion. Significance is determined by t test.

In addition to changes in polymerization and depolymerization, we identified other parameters that exhibit strong dependence on temperature. To determine how catastrophe is impacted by temperature change, we measured the length that a microtubule as-sembles before a catastrophe event and found that these assembly lengths decrease as temperature decreases (Figure 1G; Table 1). In other words, at lower temperatures, less lattice is assembled before the microtubule undergoes catastrophe. We find that at 10°C, 15 of

	Polymerization (μm/min)	Depolymerization (μm/min)	Polymerization length before catastrophe (μm)	Dynamicity (subunits/s)
10°C (n = 23)	0.62 ± 0.16 n = 20	0.57 ± 0.16 n = 29	0.50 ± 0.21	13.80 ± 2.80
25°C (n = 21)	0.91 ± 0.12 n = 47	1.36 ± 0.16 n = 49	0.81 ± 0.17	25.98 ± 2.47
30°C (n = 30)	1.15 ± 0.07 n = 104	1.94 ± 0.15 n = 101	1.01 ± 0.18	35.25 ± 1.89
37°C (n = 22)	1.59 ± 0.11 n = 102	3.01 ± 0.23 n = 97	1.23 ± 0.21	51.07 ± 5.82
39°C (n = 11)	1.59 ± 0.18 n = 53	2.95 ± 0.29 n = 51		49.48 ± 5.41

TABLE 1: Microtubule dynamics across temperatures. Values are mean ± 95%CI.

17 catastrophe events lead to a complete loss of the microtubule. Indeed, the scarcity of rescue events at 10°C and 25°C does not permit a reliable measurement of rescue frequency. At these lower temperatures, microtubules tend to depolymerize below our resolution limit (0.213 μm) and cannot be distinguished from the spindle pole bodies (SPBs; the microtubule organizing centers in budding yeast). We also measured dynamicity, defined as the overall exchange of tubulin dimers at the microtubule end per second (Jordan et al., 1993). We found that dynamicity decreases significantly as the temperature lowers from 37°C to 10°C (Table 1).

We next examined how temperature impacts the formation of microtubules from nucleation sites at the SPBs. We identified astral microtubules that depolymerized to lengths below the resolution limit of our microscope (0.213 μm) and measured the time elapsed before an astral microtubule re-emerged from the SPB (Figure 1H). At lower temperatures, we observed significant delays before re-emergence (Figure 1I; 10°C). Figure 1H depicts the frequency of astral microtubules that emerged from the SPB within 20 s of depolymerizing below our resolution limit; we termed this "refire frequency." This analysis shows that low temperature reduces astral microtubule emergence from the SPB (Figure 1I; Supplemental Figure S1). In fact, these data may underrepresent the impact of low temperature. We find that at 10°C, 7 of 22 cells failed to form new astral microtubules within the 10-min time frame of our analysis compared with 0 of 30 cells at 30°C and 1 of 21 cells at 37°C. These results suggest that failure to initiate microtubule formation at nucleation sites may contribute to the loss of microtubule polymer at low temperature.

αβ-tubulin levels are maintained at low temperature despite loss of microtubules

Because microtubule polymerization rate depends on the concentration of αβ-tubulin heterodimers, we next tested whether the loss of microtubules at low temperature could be attributable to cold-induced destruction of αβ-tubulin heterodimers. Previous work in human neuronal cell lines and iPSC-derived neurons has shown that exposure to low temperatures causes a loss of microtubule polymer as well as a decrease in tubulin protein levels (Huff et al., 2010; Ou et al., 2018). To determine if budding yeast has the same response to low temperatures, we examined microtubules and αβ-tubulin protein levels in cells after prolonged exposure to low temperature. Cells grown to early log phase at 30°C and then shifted to 4°C lost all astral microtubules within 15 min, and this loss of polymer persisted after 24 h at 4°C (Figure 2, A and B). Nuclear microtubule loss was more gradual than astral microtubules, but after 60 min at 4°C,

most cells lacked both astral and nuclear microtubules. In contrast to the loss of microtubule polymer, we found no change in tubulin protein levels, based on Western blots for α-tubulin and β-tubulin in lysates from cells incubated at 30°C or 4°C for 24 h (Figure 2C). As a second test of whether tubulin irreversibly loses activity during prolonged exposure to low temperature, we measured the kinetics of astral microtubule recovery after shifting cells from 4°C back to 30°C (Figure 2D). We found that astral microtubules recover quickly, on a time scale of seconds, when cells are shifted back to 30°C (Figure 2E). This indicates that αβ-tubulin can quickly recover polymerization activity when the temperature is raised. The rapid time scale also suggests that it is unlikely that recovery requires the biogenesis of a new pool of tubulin at 30°C, which occurs on the order of minutes (J.M., unpublished data). These results suggest that low temperature inhibits microtubule assembly without depleting the levels of tubulin protein in the cell.

Filamentous actin is not lost at low temperature

Low temperature is expected to generally slow biochemical reactions and have pervasive effects on cellular homeostasis that could indirectly inhibit microtubule assembly. To assess whether cytoskeletal dynamics are generally diminished at low temperatures, we examined the effects on the actin cytoskeleton. We measured F-actin polymerization and depolymerization across temperatures using the well-established model of endocytic patch dynamics in budding yeast (Lin et al., 2010). We labeled F-actin using Lifeact-GFP and recorded time-lapse images on a spinning disk confocal microscope at 10°C and 37°C (Figure 3A). The lifetimes of actin patches are longer at 10°C compared with 37°C (29.92 ± 2.72 s at 10°C, n = 49; 7.08, ± 0.786 s at 37°C, n = 30; p < 0.0001; Figure 3, A and B). Furthermore, the rates at which the intensity of Lifeact-GFP at individual patches increase and decrease, indicative of F-actin polymerization and depolymerization, are slower at 10°C compared with 37°C (Figure 3C). These slower rates are reminiscent of the effects we measured for microtubule dynamics. However, an important difference is that cells do not lose F-actin polymer at low temperatures. We shifted cells to 4°C for up to 24 h and found that actin patches and cables are still present (Figure 3D). We conclude that actin dynamics slow at low temperatures, but unlike microtubules, F-actin is not lost.

Tubulin chaperones help recycle tubulin at low temperatures

We hypothesize that low temperature may trap tubulin in an assembly-incompetent state, such as the cold-induced oligomers seen in vitro (Bordas et al., 1983; Lange et al., 1988; Mandelkow et al., 1991), and factors that bind tubulin could play a role in recycling a
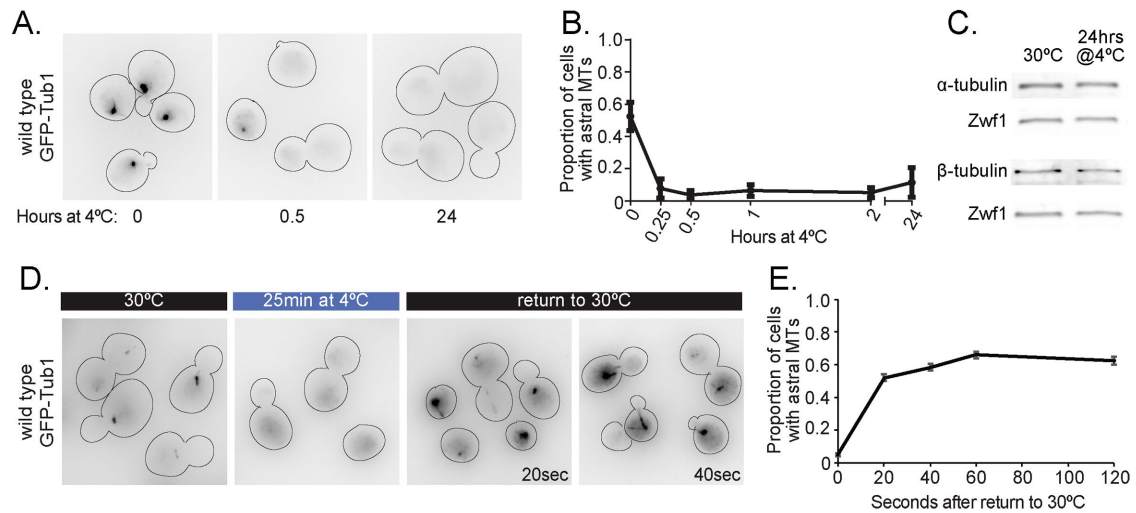
FIGURE 2: αβ-tubulin levels are maintained at low temperature despite the loss of microtubules. (A) Representative field of wild-type cells expressing GFP-Tub1 shifted from 30°C to 4°C for 0, 0.5, and 24 h. These images use an inverted lookup table to enhance contrast for the GFP-Tub1 signal. (B) Proportion of wild-type cells with astral microtubules present after shifting to 4°C for indicated time. Values are mean ± SEM from at least three separate experiments with at least 420 cells analyzed for each timepoint. (C) Western blot of protein lysate from wild-type cells incubated at 30°C and at 4°C for 24 h, probed for α-tubulin, β-tubulin, and Zwf1 (Glucose-6-phosphate dehydrogenase). (D) Representative field of wild-type cells expressing GFP-Tub1 incubated at 30°C, 25 min after shifting to 4°C, and 20 and 40 s after shifting back to 30°C from 4°C. (E) Proportion of wild-type cells with astral microtubules present after shifting from 4°C to 30°C for indicated time. Each data point represents a proportion calculated from data pooled from three separate experiments with at least 482 cells analyzed for each timepoint. Error bars are standard error of proportion.

heterodimer back to an assembly-competent state. We sought to use cold sensitivity to identify cellular mechanisms for recycling assembly-incompetent tubulin by screening null alleles for a cold-sensitive phenotype. We hypothesized that cells might co-opt tubulin biogenesis pathways to maintain the pool of assembly-competent tubulin (Figure 4A), and that this role may become more important at lower temperatures. To test this, we systematically generated all viable null mutants in the tubulin biogenesis pathway and screened for growth defects at low temperature (Figure 4, B and C). We also

screened mutations known to regulate microtubule dynamics and motor activity (Supplemental Figure S2). To distinguish growth defects that are specific to cold sensitivity from those caused by general depletion of assembly-competent heterodimers, we also tested each mutant for sensitivity to the destabilizing drug benomyl (Figure 4, B and C; Supplemental Figure S2). We found that null mutants in the prefoldin complex components *GIM3*, *GIM5*, and *YKE2* impair growth at 15°C compared with wild-type controls, but also exhibit hypersensitivity to benomyl (Figure 4B). Although null mutants in
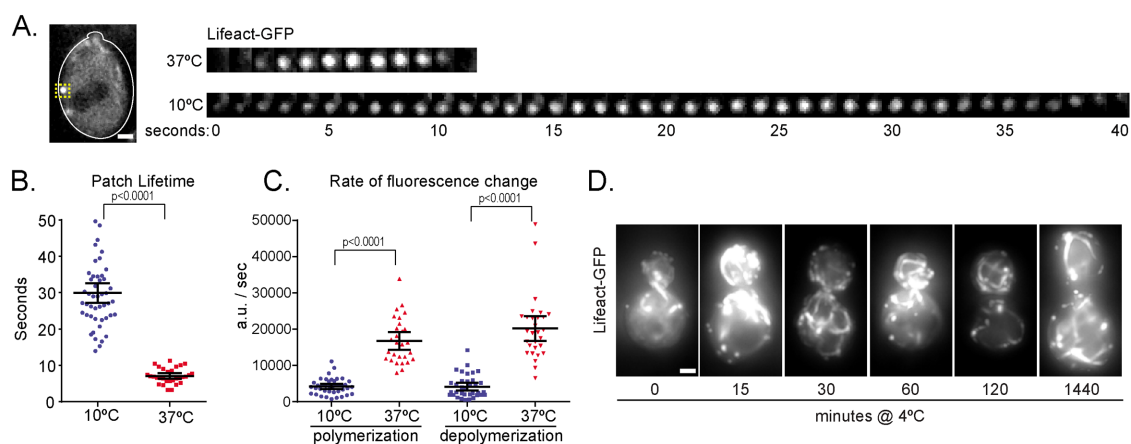

FIGURE 3: Filamentous actin is not lost at low temperature. (A) Image of example wild-type cell expressing Lifeact-GFP with yellow box labeling an actin patch (left). Scale bar, 1 μm. Image series of zoomed in actin patch at 37°C (top) and 10°C (bottom) imaged at 1-s intervals (right). (B) Actin patch lifetime measured by the full-width at ¾ maximum intensity of the actin patch curve at 10°C (blue) and 37°C (red); *n* = 49 cells at 10°C; *n* = 30 cells at 37°C; values are mean with 95% CI. (C) Rates of actin patch polymerization and depolymerization at 10°C (blue) and 37°C (red); *n* = 39 polymerization and 36 depolymerization events at 10°C; *n* = 28 polymerization and 29 depolymerization events at 37°C; values are mean with 95% CI. (D) Images series of wild-type cells expressing Lifeact-GFP shifted from 30°C to 4°C for the number of minutes indicated below. Scale bar, 1 μm.
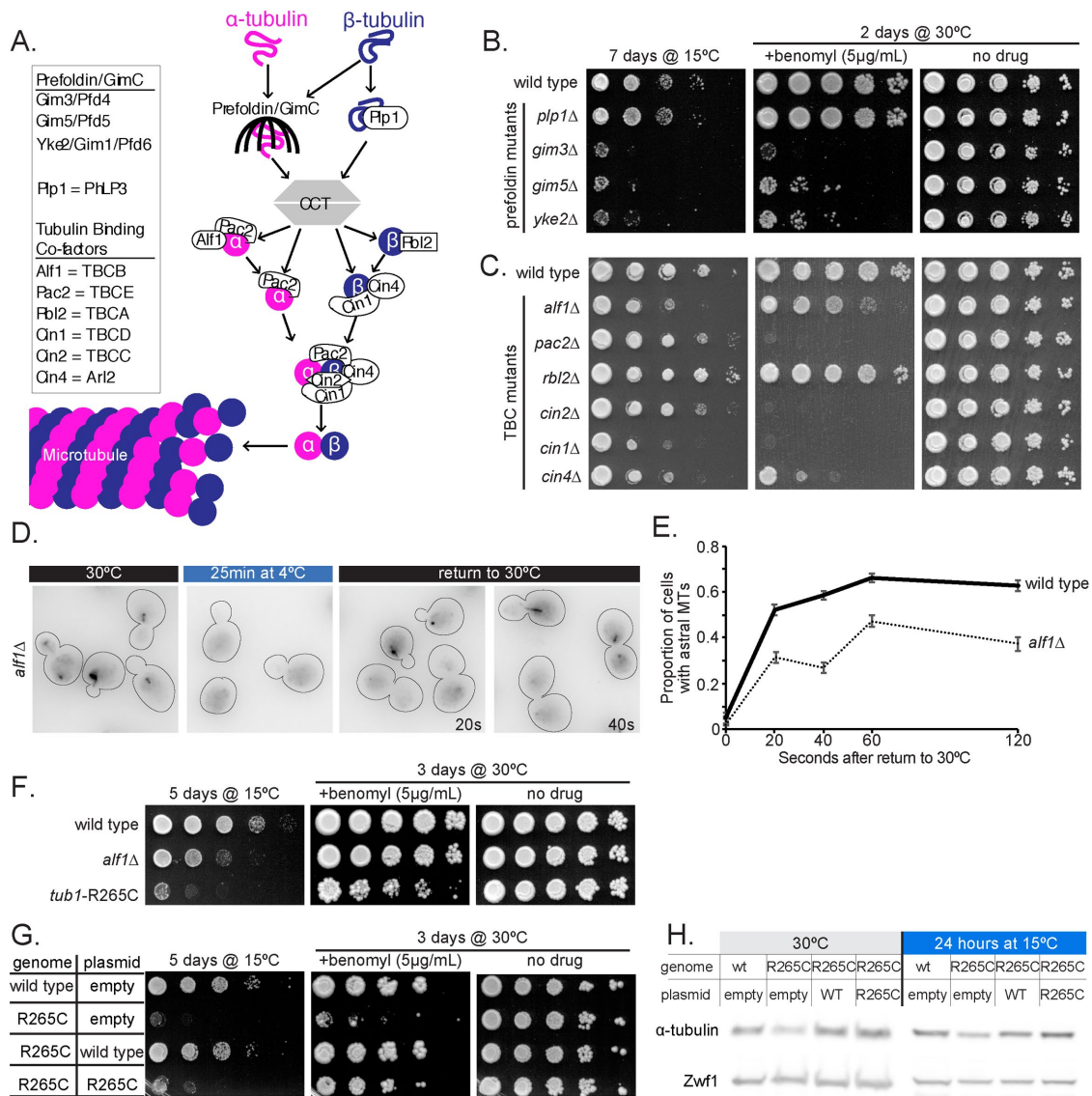
FIGURE 4: Tubulin chaperones help recycle tubulin at low temperatures. (A) Model of the tubulin biogenesis pathway (adapted from Nithianantham *et al.*, 2015; Tian *et al.*, 1997). (B, C) Tenfold dilution series of null strains for the prefoldin (B), CCT (B), and TBCs (C) indicated at left were spotted to rich medium or rich medium supplemented with 5 µg/ml benomyl and grown at the indicated temperature for the indicated time. (D) Representative field of *alf1Δ* cells expressing GFP-Tub1 incubated at 30°C, 25 min after shifting to 4°C, and 20 and 40 s after shifting back to 30°C from 4°C. (E) Proportion of wild-type (solid line) and *alf1Δ* (dotted line) with astral microtubules present after shifting from 4°C to 30°C for the indicated time. Each data point represents a proportion calculated from data pooled from three separate experiments with at least 266 cells analyzed for each timepoint. Error bars are standard error of proportion. (F) Tenfold dilution series of strain indicated at left were spotted to rich medium or rich medium supplemented with 5 µg/ml benomyl and grown at the indicated temperature for the indicated time. (G) Tenfold dilution series of strain carrying the plasmid indicated at left were spotted to rich medium or rich medium supplemented with 5 µg/ml benomyl and grown at the indicated temperature for the indicated time. (H) Western blot of protein lysate from wild-type or tub1-R265C cells carrying the indicated plasmid incubated at 30°C or 15°C for 24 h and probed for α-tubulin and Zwf1.

most CCT genes are lethal in yeast, we did test a null mutant in *PLP1* (Lacefield and Solomon, 2003), but found that this has little to no phenotype at low temperature or in the presence of benomyl (Figure 4B). Several null mutants in the TBC genes showed sensitivity to low temperature and benomyl; however, the null mutant in *ALF1/TBCB* showed increased cold sensitivity but only slightly increased benomyl sensitivity compared with wild-type controls (Figure 4C). We therefore prioritized the *ALF1/TBCB* null mutant for further study. Our analysis also identified increased cold sensitivity

for null mutants in the microtubule regulators *BIK1*/CLIP170, *BIM1*/EB1 and *CIN8*/kinesin-5 (Supplemental Figure S2).

We used a series of experiments to investigate how loss of *ALF1/TBCB* impacts tubulin activity. We first tested the possibility that Alf1 protein levels increase on exposure to low temperatures; however, we found that Alf1 levels remain constant, even after prolonged exposure to low temperature (Supplemental Figure S3, A and B). Next, we sought to examine microtubule dynamics in *alf1Δ* null mutants. We created an alf1Δ null mutant strain that expresses GFP-Tub1;

	Polymerization (μm/min)	Depolymerization (μm/min)	Catastrophe frequency (events/min)	Dynamicity (subunits/s)
WT 30°C (*n* = 21)	1.48 ± 0.12 *n* = 104	2.41 ± 0.20 *n* = 88	0.73 ± 0.13 *n* = 17	44.27 ± 2.98
alf1Δ 30°C (*n* = 21)	1.40 ± 0.10 *n* = 92	2.38 ± 0.19 *n* = 89	0.70 ± 0.12 *n* = 18	44.04 ± 1.64

TABLE 2: Microtubule dynamics using Bik1-3GFP. Values are mean ± 95%CI.

however, we found that GFP-Tub1 signal bleaches more rapidly in these cells than in wild-type cells. This does not appear to be due to lower expression of GFP-Tub1 in *alf1Δ* mutants, based on Western blotting (Supplemental Figure S3C), and may therefore reflect a loss of assembly activity for the GFP-Tub1 fusion when cells lack Alf1/TBCB. To circumvent this issue, we created strains expressing Bik1/CLIP170 fused to 3GFP to label microtubule ends. Time-lapse imaging of Bik1-3GFP in *alf1Δ* cells and wild-type controls showed no differences in polymerization rates or other parameters of microtubule dynamics at 30°C (Table 2). This suggests that tubulin activity is not diminished in *alf1Δ* mutant cells at 30°C. We next measured the effect of low temperature. When incubated at 4°C for 25 min before increasing the temperature back to 30°C, *alf1Δ* mutant cells exhibit slower recovery of astral microtubules than wild-type cells (Figure 4, D and E). This slower recovery of astral microtubules in the *alf1Δ* mutant happens on a time scale that is faster than would be expected for the biogenesis of new tubulin. Accordingly, this suggests that Alf1 promotes the recovery of tubulin assembly competence after cold-induced depolymerization.

To further investigate a role for Alf1/TBCB in tubulin recycling, we used an α-tubulin mutation, R264C, that was originally identified through association with human brain malformations and subsequently shown to disrupt its interaction with TBCB (Tian *et al.*, 2008). We generated an analogous mutation at the R265 residue in the major yeast α-tubulin, *TUB1*. We find that *tub1*-R265C mutant cells exhibit a level of cold sensitivity that is similar to *alf1Δ* null mutants (Figure 4F). However, *tub1*-R265C mutants are more sensitive to benomyl than *alf1Δ* null mutants (Figure 4F). Providing cells with an additional copy of the *tub1*-R265C mutant allele rescues benomyl sensitivity, but not cold sensitivity (Figure 4, G and H). This suggests the interaction between tubulin and the Alf1/TBCB becomes essential at low temperature. We also sought to directly measure the assembly activity of R265C mutant tubulin by fusing it to GFP; however, the fusion did not localize to microtubules (unpublished data). This result is reminiscent of our findings when expressing wild-type GFP-Tub1 in *alf1Δ* mutants and suggests that the GFP fusion to α-tubulin may exacerbate the effect of losing Alf1/TBCB. Together, these data support our hypothesis that the tubulin biogenesis pathway plays a role in recycling tubulin to replenish the assembly-competent pool.

Preventing tubulin maturation stabilizes microtubules at low temperatures

As a second test of our hypothesis that low temperature traps tubulin in an assembly-incompetent state, we predicted that tubulin mutants that persist in an immature, assembly-competent state could confer cold stability to microtubules. To test this prediction, we introduced a C354S substitution mutation into the β-tubulin gene, *TUB2* (Figure 5A). The tub2-C354S mutant has been previously shown to form hyperstable microtubules in vivo and in vitro, and microtubules assembled from tub2-C354S heterodimers in vitro preferentially bind to the yeast EB protein, Bim1 (Gupta *et al.*, 2001, 2002; Geyer *et al.*, 2015). Furthermore, the *tub2*-C354S mutant

exhibits resistance to benomyl (Gupta *et al.*, 2001). Based on these results, this mutation is thought to block heterodimer compaction associated with GTP hydrolysis and therefore remain in a constitutively immature, assembly-competent state (Geyer *et al.*, 2015). Consistent with previous studies, we find that cells expressing tub2-C354S exhibit persistent astral microtubules after shifting to 4°C (Figure 5B). These astral microtubules persist even after incubating mutant cells for 24 h at 4°C (Figure 5C). In our microtubule dynamics assay, we find that tub2-C354S slows microtubule polymerization and depolymerization and exhibits fewer catastrophes and rescues than wild-type cells across temperatures from 10°C to 37°C (Figure 5D) This is consistent with previously published studies of the *tub2*-C354S mutant, which were conducted at 23°C (Gupta *et al.*, 2002). At low temperature (10°C), tub2-C354S microtubules exhibit little change in length over time, indicating that the cold stability of the mutant tubulin is not attributable to faster assembly rates (Figure 5D). To test whether the cold stability of tub2-C354S mutant tubulin could be explained by increased tubulin concentration, we measured αβ-tubulin levels via Western blot and found that wild-type and *tub2*-C354S cells maintain similar amounts of tubulin across temperatures (Figure 5E). Thus, maintaining tubulin in an assembly-competent state is sufficient to stabilize microtubules at low temperature.

tub2-C354S rescues the cold sensitivity of *alf1Δ*

Together, our data support a model in which low temperature traps tubulin in an assembly-incompetent state, and that the tubulin biogenesis pathway may help tubulin escape and return to the assembly-competent state. Based on this model, we predict that the *tub2*-C354S mutation should rescue the requirement for *ALF1*/TBCB at low temperatures by keeping tubulin in an assembly-competent state. To test this prediction, we directly assessed microtubule stability at low temperatures. We used a modified version of our cold-shift experiment—instead of incubating cells at 4°C, where wild-type cells lose all microtubule polymer, we used an intermediate temperature of 15°C and analyzed the portion of cells with remaining GFP–Tub1-labeled astral microtubules (Figure 6A). We find that *tub2*-C354S *alf1Δ* double mutants have a higher frequency of cells with astral microtubules than wild-type controls or the *alf1Δ* single mutant but decreased compared with the *tub2*-C354S single mutant after 120 min at 15°C (Figure 6B). We confirmed by Western blot that all strains used in this experiment have similar tubulin concentrations, and that these concentrations are not altered by shifting to low temperature (Figure 6C). Therefore, the *tub2*-C354S mutation rescues the loss of *ALF1*/TBCB by restoring the quality of the tubulin pool, not the quantity. These results add support to our model that Alf1/TBCB promotes the return of tubulin to an assembly-competent state.

DISCUSSION

The cold sensitivity of microtubules has been known for many years. In early studies, cold sensitivity distinguished microtubules from
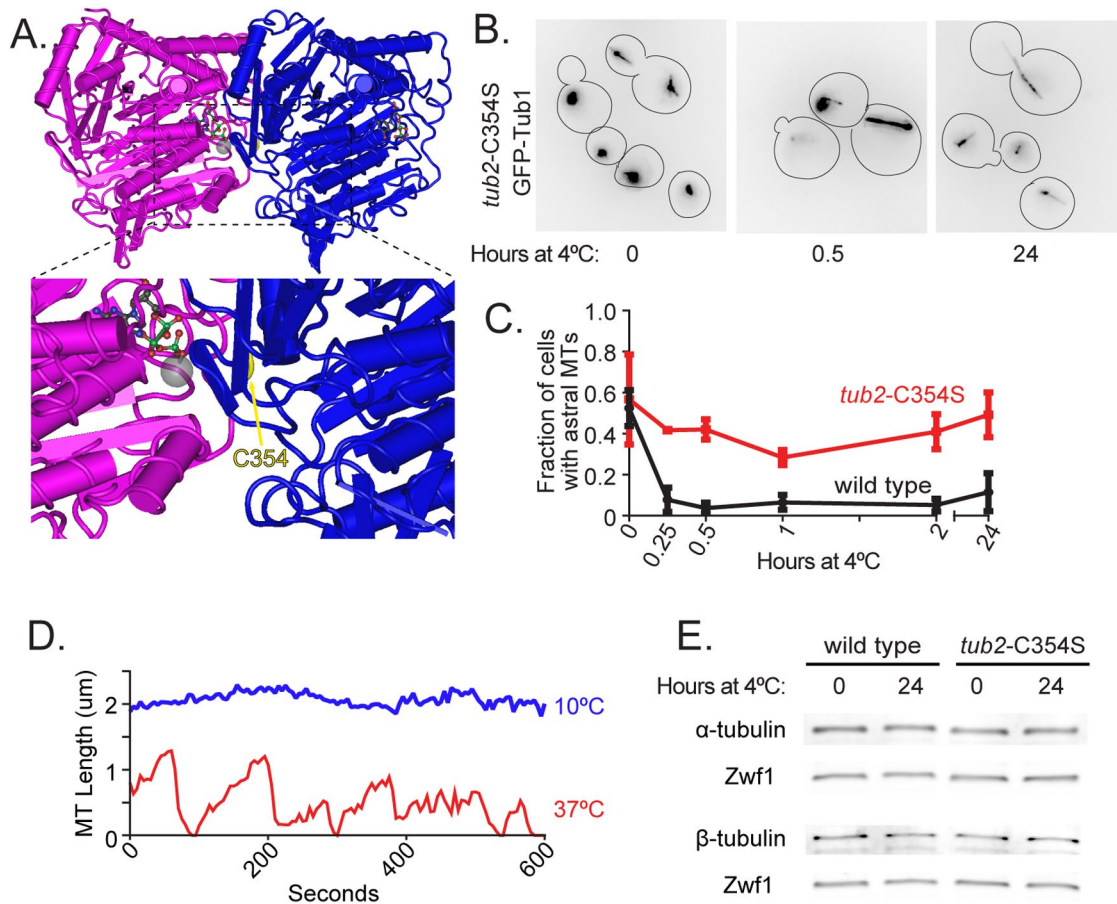
FIGURE 5: Preventing tubulin maturation stabilizes microtubules at low temperatures. (A) Model of tubulin heterodimer with arrow pointing to residue C354 on β-tubulin (PDB entry 5W3H; Howes *et al.*, 2017). (B) Representative field of tub2-C354S cells expressing GFP-Tub1 shifted from 30°C to 4°C for 0, 0.5, and 24 h. These images use an inverted lookup table to enhance contrast for the GFP-Tub1 signal. (C) Proportion of wild-type (black) and tub2-C354S (red) cells with astral microtubules present after shifting to 4°C for indicated time. Values are mean ± SEM from at least three separate experiments with at least 420 cells analyzed for each timepoint. (D) Lifeplots of a single tub2-C354S astral microtubule at 10°C (blue) and 37°C (red). Microtubule lengths were measured at 5-s intervals. (E) Western blot of protein lysate from wild-type (left) and tub2-C354S (right) cells incubated at 30°C and at 4°C for 24 h and probed for α-tubulin, β-tubulin, and Zwf1.

other cytoskeletal filaments, and it has since been used as a tool to selectively disrupt microtubule networks in cells and to purify tubulin from cells through cycles of temperature-induced depolymerization and polymerization (Tilney and Porter, 1967; Olmsted *et al.*, 1974; Inoué, 2010). Although cold sensitivity is well known, why cells lose microtubules at low temperatures has not been precisely defined. The goals of this study are to define the mechanistic basis for microtubule loss at low temperatures and then to use this as a tool to gain broader insight into how cells regulate microtubule dynamics.

An important question is whether microtubule loss at low temperature is attributable to direct effects on tubulin activity or indirect consequences of temperature-induced changes in cell physiology. While we cannot completely rule out the impact of other cold-induced changes in cell physiology, several lines of evidence indicate that microtubule loss results from direct effects on tubulin activity. It is well established that the activity of purified tubulin exhibits strong dependence on temperature. Microtubules reconstituted in vitro from purified mammalian tubulin are destabilized by low temperature and exhibit unique, curled protofilament architectures that suggest temperature-dependent changes in inter- and/or intraheterodimer interactions (Mandelkow *et al.*, 1991). Interestingly, tubulin

purified from psychrophilic organisms forms microtubules that remain stable at low temperature, consistent with the notion that interspecies differences in the tubulin proteins may determine cold sensitivity (Himes and Detrich, 1989). Thus, temperature directly and potently impacts the tubulin protein in a way that alters its assembly activity. By comparison, F-actin reconstituted in vitro from purified mammalian actin is not destabilized by low temperature (Weber *et al.*, 1975; Breton and Brown, 1998). We also find F-actin in yeast cells is not lost at low temperatures (Figure 3). Although the rates of F-actin polymerization and depolymerization do slow when temperature decreases to 10°C, there is no net loss of F-actin, even after prolonged exposure to 4°C (Figure 3C). Thus, polymer loss at low temperature is a unique feature of tubulin and likely due to temperature-dependent effects on protein activity.

In seeking to define the mechanistic basis for microtubule loss at low temperatures, we first considered a simple kinetic model in which changes in four parameters of microtubule dynamics—polymerization rate, depolymerization rate, catastrophe frequency, and rescue frequency—would be sufficient to explain microtubule loss at low temperatures. We find that both polymerization and depolymerization rates decrease as the temperature decreases from
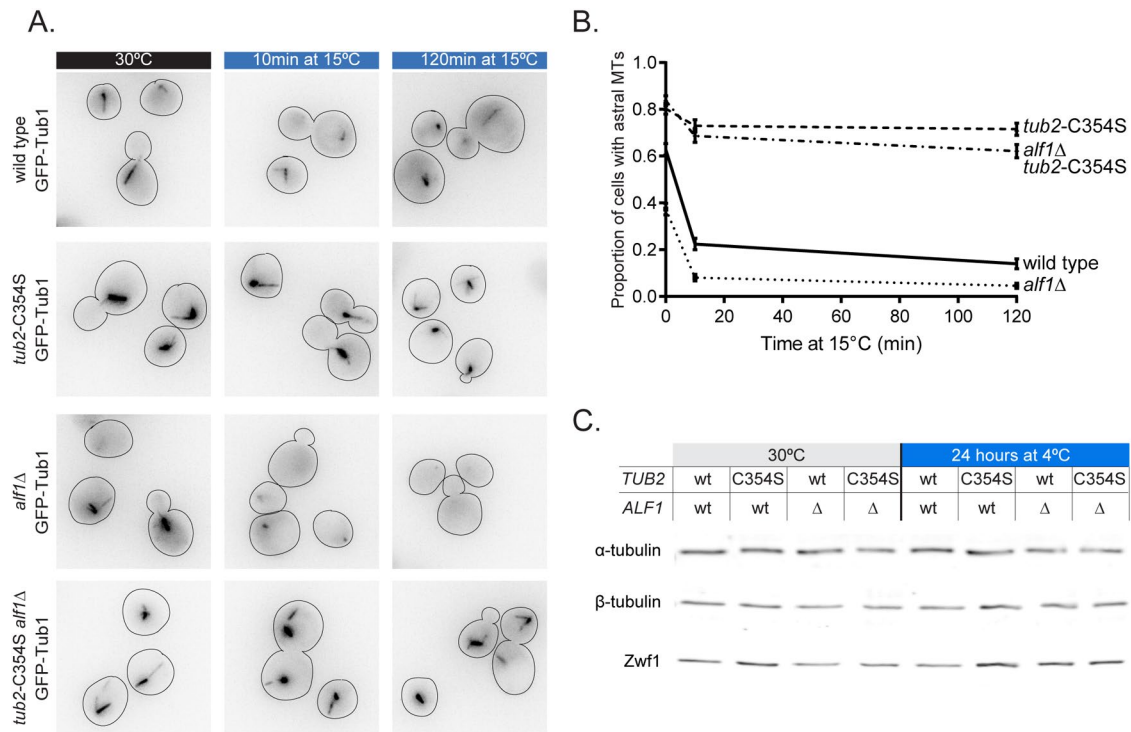
FIGURE 6: *tub2*-C354S rescues the cold sensitivity of *alf1*Δ. (A) Representative field of wild-type, *alf1*Δ, tub2-C354S, and *alf1*Δ with tub2-C354S cells expressing GFP-Tub1 after 20 min at 30°C, 10 min after shifting to 15°C, and 120 min after shifting to 15°C. (B) Proportion of wild-type (solid line), *alf1*Δ (dotted line), tub2-C354S (dashed line), and *alf1*Δ with tub2-C354S (dot-dashed line) cells with astral microtubules present after shifting from 30°C to 15°C for the indicated time. Each data point represents a proportion calculated from data pooled from three separate experiments with at least 293 cells analyzed for each timepoint. Error bars are standard error of proportion. (C) Western blot of protein lysate from wild-type and tub2-C354S cells with or without Alf1 incubated at 30°C and at 4°C for 24 h and probed for α-tubulin, β-tubulin, and Zwf1.

37°C and 10°C (Figure 1; Table 1) consistent with what has been observed in vitro (Fygenson *et al.*, 1994). Surprisingly, the effect of temperature on depolymerization rate is more pronounced than what we observed for polymerization rate. The Arrhenius plot in Figure 1F shows these rates intersecting at ~13°C, and at lower temperatures the polymerization rate is faster than the depolymerization rate. Although polymerization and depolymerization are clearly impacted by temperature change, we conclude that these effects alone are not sufficient to explain the loss of microtubule polymer at low temperatures. We did not observe enough rescue events at 10°C and 25°C to make reliable measurements; however, we did find that catastrophe frequency increases at low temperature. Since polymerization slows as temperature decreases, we measured catastrophe as a function of microtubule length assembled, rather than as a function of time. We find that this length value decreases as the temperature lowers (Figure 1; Table 1). Thus, at low temperatures, less microtubule lattice is assembled before catastrophe occurs. We propose two models that could explain how low temperature promotes catastrophe. In the first model, the slower rate of tubulin addition to the plus end at low temperatures may not outpace GTP hydrolysis. Accordingly, plus ends may have shorter GTP caps at low temperatures. In the second model, low temperature may destabilize the plus end by inhibiting lateral interactions between protofilaments. This model is inspired by recent observations that assembling plus ends contains protofilament extensions that must zipper together to form a complete lattice (McIntosh *et al.*, 2018) and older evidence that low temperature induces protofilaments to adopt an outwardly curled configuration that prevents

lateral interactions (Mandelkow *et al.*, 1991). In either of our models, the loss of microtubule polymer at lower temperatures may be explained by increased catastrophes.

In addition to increasing catastrophe frequency, our results also suggest that low temperature reduces microtubule nucleation activity. We find that low temperature reduces the emergence of microtubules from SPBs (Figure 1, H and I). Since SPBs contain γ-tubulin small complexes (γ-TuSCs) that nucleate microtubules, this effect could be attributable to cold sensitivity of γ-TuSC activity and/or the intrinsic nucleation activity of αβ-tubulin heterodimers (Sobel and Snyder, 1995; Zheng *et al.*, 1995). Thus, the loss of microtubules at low temperatures may be explained by depolymerization back to the SPB and failure to nucleate new microtubules. Although our results do not clearly distinguish whether decreased nucleation activity or increased catastrophe frequency contributes more strongly to microtubule loss at low temperatures, an intriguing possibility is that these two may be linked. Importantly, our refiring assay does not resolve whether microtubules fail to nucleate or newly nucleated microtubules catastrophe before reaching a length that is sufficient for visualization.

We speculate that the formation of assembly-incompetent tubulin may be a pervasive feature of microtubule dynamics that is exacerbated by, rather than unique to, low temperature. Numerous in vitro reconstitution studies have shown that depolymerized tubulin is intrinsically capable of cycling back to an assembly-competent, GTP-bound state when provided with optimal conditions. These conditions include warm temperatures, high concentrations of free GTP (1 mM), 80 mM PIPES, high Mg^{2+} (≥1 mM), and low Ca^{2+}

(Weisenberg, 1972; Borisy *et al.*, 1975; Lee and Timasheff, 1977). How this transition from assembly-incompetent, GDP-tubulin to assembly-competent, GTP-tubulin is achieved in a complex in vivo cellular environment is an important question. Conditions in cells differ from in vitro reconstitution experiments in ways that are likely to impact tubulin activity. For example, consider budding yeast in which the total intracellular concentration of GTP is reported to be 1.5 mM (Breton *et al.,* 2008) with many proteins competing with tubulin for binding to this nucleotide pool. Intracellular Mg^{2+} ranges between 500 µM and 1 mM (Romani and Scarpa, 1992), and most of these cations are complexed with proteins and nucleic acids (Cyert and Philpott, 2013). Available Mg^{2+} in vivo is therefore likely below the concentrations required for microtubule dynamics in vitro. Finally, many eukaryotic cells maintain nM concentrations of Ca^{2+} in the cytoplasm, and budding yeast can survive with cytosolic Ca^{2+} concentrations up to 2 mM (Kováč, 1985; Halachmi and Eilam, 1989); however, in vitro microtubule dynamics assays typically contain no Ca^{2+} (Gell *et al.,* 2010). Thus, the conditions that support dynamic tubulin assembly in vitro are unlikely to represent the complexity of tubulin regulation in vivo. Extrinsic factors are likely to play critical roles in regulating tubulin activity in the cellular environment.

Our results also reveal that low temperature causes tubulin to accumulate in an assembly-incompetent state that is the product of microtubule disassembly. Our confirmation of the previous finding that the C354S mutation in β-tubulin maintains microtubules at low temperature indicates that a full maturation cycle is required for tubulin to visit the assembly-incompetent state (Figure 5; Gupta *et al.,* 2001, 2002). The C354S mutation is thought to disrupt the tubulin cycle and maintain an "immature" state by uncoupling GTP hydrolysis from conformational changes (Geyer *et al.,* 2015). Accordingly, C354S mutant tubulin may not visit the assembly-incompetent state of the tubulin cycle. Importantly, we found that total tubulin concentration in yeast cells, for both wild-type and C354S mutants, does not change when temperature is decreased as low as 4°C (Figures 2E and 5D). This stands in contrast to the decrease in tubulin concentration during exposure to low temperatures that has been previously reported in cultured human neurons (Huff *et al.,* 2010; Ou *et al.,* 2018). Based on this evidence, we propose that when tubulin depolymerizes at low temperature it becomes trapped in a conformationally matured, assembly-incompetent state that is incompatible with microtubule polymerization. This model could therefore lead to microtubule loss by sequestering the pool of tubulin in the cell and contributing to slower polymerization rates observed at low temperatures.

We find that TBCs, particularly TBCB/Alf1, play an important role in recycling tubulin to maintain the pool of assembly-competent tubulin in the cell. Previous studies found that a complex of TBCB and TBCE dissolves heterodimers and forms a tripartite complex with α-tubulin (Kortazar *et al.,* 2007; Serna *et al.,* 2015). These results suggest that TBCB acts not only on α-tubulin monomers during tubulin biogenesis but also on formed αβ-tubulin heterodimers as well. The relevance of this activity in cells has not been established, but it can be speculated that heterodimer dissolving activity could be involved in heterodimer quality control or recycling. We find that disrupting TBCB/Alf1 further sensitizes cells to low temperatures and delays the recovery of microtubule polymerization after cold shock. Disrupting TBCB/Alf1 does not detectably diminish the levels of α- or β-tubulin or change the dynamicity or catastrophe frequency of microtubules at 30°C (Figure 4; Table 2). The latter point is important because TBCB/Alf1 contains a CAP-Gly domain that is also found in the microtubule-binding proteins Bik1/CLIP170 and

Nip100/p150[glued]. Blocking α-tubulin from interacting with TBCB/Alf1 with the R265C mutation also sensitizes cells to cold temperatures, and this sensitivity is not suppressed by increasing the expression of the R265C mutant α-tubulin (Figure 4). One possible model to explain the importance of TBCB/Alf1 at low temperatures is that it might be triggered by decreasing temperature, similar to what has been shown for "cold-responsive" genes in yeast and other organisms (Aguilera *et al.,* 2007). However, previous transcriptome analysis of *Saccharomyces cerevisiae* during cold shock did not reveal increases in TBCB/Alf1 expression or other TBCs (Abe, 2007), and we found no change in Alf1 levels after a shift to low temperatures (Supplemental Figure S3A). Instead, we propose TBCB generally promotes the recycling of tubulin from an assembly-incompetent to an assembly-competent state, and that this maintenance of the tubulin pool becomes essential under microtubule-destabilizing conditions, such as low temperatures. How TBCs might inhibit or resolve the assembly-incompetent state, and whether this role extends to other stress conditions, are important questions for further study.

Finally, our work highlights a critical role for tubulin in determining the fitness of organisms at low temperature. Interestingly, our results indicate that the cold sensitivity of wild-type yeast cells may not be primarily due to mitotic spindle defects. We find that cells released from G1 synchronization at 15°C form bipolar spindles and enter anaphase with kinetics that are indistinguishable from mutants deficient for spindle assembly checkpoint activity (*mad2Δ*), but significantly faster than cells treated with microtubule-destabilizing drugs (Supplemental Figure S4, B and C). Furthermore, the growth rate of *mad2Δ* mutant cells at low temperatures is similar to wild-type controls (Supplemental Figure S4). This raises the possibility that the loss of microtubules at low temperatures impairs fitness through a mechanism that is separate from mitotic progression. One possibility is that increasing the pool of assembly-incompetent tubulin in the cytoplasm triggers a secondary stress response that slows proliferation. This hypothesis will be the focus of further investigation.

MATERIALS AND METHODS

Yeast strains, manipulations, and plasmid construction

General yeast manipulation, media, and transformation were performed by standard methods (Amberg *et al.,* 2000). A detailed list of strains and plasmids is provided in Tables S1 and S2. GFP-Tub1 fusions were integrated at the *LEU2* locus and expressed ectopically, in addition to the native *TUB1* (Song and Lee, 2001). Spc110-tdTomato was generated using conventional methods and expressed from the genomic locus (Sheff and Thorn, 2004). The tub2-C354S mutation to *TUB2* was made at the native chromosomal locus as previously described (Aiken *et al.,* 2014) and confirmed by sequencing. Deletion mutants were generated by conventional methods (Petracek and Longtine, 2002). A fragment of the TUB1 gene including the open reading frame (with intron), 992 base pairs of 5' UTR, and 487 base pairs of 3' UTR was amplified from the genomic DNA by PCR. This fragment was cloned into the plasmid pRS314 (Sikorski and Hieter, 1989) using sticky end cloning with *Not*I and *Kpn*I sites and confirmed by sequencing to yield plasmid pJM267. QuikChange Lightning Site-Directed Mutagenesis Kit (Agilent Technologies; Santa Clara, CA) was used to introduce the tub1-R265C mutation to pJM267 (Aiken *et al.,* 2019).

Microtubule dynamics in living cells

Images were collected on a Nikon Ti-E microscope equipped with a 1.45 NA 100 × CFI Plan Apo objective, piezo electric stage (Physik Instrumente, Auburn, MA), spinning disk confocal scanner unit (CSU10; Yokogawa), 488-nm laser (Agilent Technologies, Santa

Clara, CA), and an EMCCD camera (iXon Ultra 897, Andor Technology, Belfast, UK) using NIS Elements software (Nikon). Cells were grown asynchronously to early log phase in nonfluorescent media and adhered to coverslips coated with concanavalin A (Fees et al., 2017). Imaging was performed at the indicated temperature using the CherryTemp temperature controller system (CherryBiotech, Rennes, France).

Microtubule dynamics were analyzed by measuring the lengths of astral microtubules labeled with GFP-Tub1 or Bik1-3GFP at 5-s intervals for 10 min. A 6.0-μm stack with a step size of 0.45 μm was taken at each timepoint and analyzed as a 2D maximum intensity projection (ImageJ, Wayne Rasband, National Institutes of Health [NIH]). Length measurements were taken for each frame beginning at the outside edge of the SPB to the tip of the astral microtubule; therefore, any movement of the SPB would not impact microtubule length measurement. All analyses were conducted in preanaphase cells. Assembly and disassembly events were defined as at least three contiguous data points that produced a length change ≥0.5 μm for 25°C, 30°C, and 37°C with a coefficient of determination ≥0.8. For experiments at 10°C, we adjusted the threshold for length change to ≥0.28 μm; however, it should be noted that nearly all depolymerization events at 10°C resulted in complete loss of the microtubule. Microtubule dynamicity was calculated by the total change in length (growing and shrinking) divided by the change in time and expressed in tubulin subunits changed per second (Jordan et al., 1993). The length of polymerization before a catastrophe event was calculated by determining the total length of polymerization before a switch to depolymerization. Catastrophe frequency was determined for individual astral microtubules by dividing the number of catastrophe events by the total lifetime of the microtubule, minus time spent in disassembly. Median microtubule length was determined from time-lapse imaging of individual astral microtubules over 10 min. Dynamics measurements for individual microtubules were pooled for each temperature and then compared with pooled data for different temperatures. Student's t test was used to assess whether the mean values for different datasets were significantly different (Fees et al., 2017). Arrhenius plot was generated by converting the polymerization and depolymerization rates from μm/min to heterodimers/s, assuming that 1 μm of yeast microtubule contains 1625 tubulin heterodimers.

Refire frequency was calculated as the proportion of astral microtubules that depolymerize to a length below our level of detection (<0.213 μm) and then polymerized to a measurable microtubule length (>0.213 μm) within 20 s (4 frames in our analysis), divided by the total number of astral microtubules that depolymerize to a length below our level of detection. At least 21 astral microtubules were analyzed for each temperature.

Microtubule loss at 4°C
Cells expressing GFP-Tub1 were grown overnight in rich liquid media in a shaking incubator at 30°C for ~16 h, diluted 1:150, and grown to early log phase in fresh media. The cultures were then shifted to a shaking incubator at 4°C for the indicated amount of time. Cells were then fixed in 3.7% formaldehyde and 0.1 M KPO$_4$ and incubated at 4°C for 3 min. Cells were then pelleted, the supernatant was removed, and the cells were suspended in quencher solution (0.1% Triton-X, 0.1 M KPO$_4$, 10 mM ethanolamine). The cells were pelleted again, and the supernatant was decanted and washed twice in 0.1 M KPO$_4$. The fixed cells were loaded into slide chambers coated with concanavalin A and washed with 0.1 M KPO$_4$ and the chambers were sealed with VALAP (Vaseline, lanolin, and paraffin at 1:1:1) (Fees and Moore, 2018).

Images were collected on a Nikon Ti-E wide field microscope equipped with a 1.49 NA 100× CFI160 Apochromat objective and an ORCA-Flash 4.0 LT sCMOS camera (Hammamatsu Photonics, Japan) using NIS Elements software (Nikon, Minato, Tokyo, Japan). Microtubules labeled with GFP-Tub1 were imaged in Z-series consisting of a 7-μm range at 0.5-μm steps, and a DIC image was taken at the equatorial plane.

Cells were segmented using a custom ImageJ macro previously described (Fees et al., 2016). The data were blinded for analysis, and the segmented cells were visually scored for the presence of astral microtubules.

Microtubule recovery assay
Cells expressing GFP-Tub1 were grown in rich liquid media in a shaking incubator at 30°C for ~16 h, then diluted 1:150 and grown to early log phase in fresh media. Culture (100 μl of each) was transferred to 200 μl PCR tubes and placed in a Bio-Rad T100 Thermal Cycler (Hercules, CA). The cells were incubated at 4°C for 35 min and warmed to 30°C for the indicated amount of time before being fixed, imaged, and analyzed for the presence of astral microtubules, as described above.

Microtubule loss at 15°C
Cells expressing GFP-Tub1 were grown in rich liquid media in a shaking incubator at 30°C for ~16 h, then diluted 1:150 and grown to early log phase in fresh media. Culture (100 μl of each) was transferred to 200 μl PCR tubes and placed in a Bio-Rad T100 Thermal Cycler (Hercules, CA). The cells were incubated at 30°C for 20 min and cooled to 15°C for the indicated amount of time before being fixed, imaged, and analyzed for the presence of astral microtubules, as described above.

Actin patch dynamics in living cells
Images were collected on a Nikon Ti-E microscope described above. Actin patch lifetime and dynamics were analyzed by measuring the accumulation and decay of Lifeact-GFP in single z-plane images acquired every 1 s for 3 min. A 0.852 μm × 0.852 μm region of interest was used to measure total fluorescence of each patch. The actin patch lifetime was defined as the amount of time the patch was ≥ ¾ of its maximum intensity by measuring the full width at ¾ maximum of the fluorescence over time. Actin patch polymerization dynamics were determined by measuring the slope of fluorescence intensity versus time from before the patch appears to the maximum intensity, and depolymerization was measured by the slope from maximum intensity to patch disappearance with a coefficient of determination ≥0.8.

Western blot
To compare tubulin protein levels before and after cold shift, cells were first grown to log phase at 30°C in 5 ml rich liquid media or selective dropout media for strains containing a plasmid, and 1 ml was removed for lysate preparation. The remaining cell culture was transferred to a platform shaking at 250 rpm at 4°C for 24 h, and then 1 ml was removed for lysate preparation. Samples were pelleted and then resuspended in 2 M lithium acetate for 5 min. The cells were then pelleted again and resuspended in 0.4 M NaOH for 5 min while on ice. Samples were then pelleted, resuspended in 70 μl of 2.5× Laemmli buffer, and boiled for 5 min. The total protein concentration of the clarified lysate was determined by Pierce 660 nm protein assay with the Ionic Detergent Compatibility Reagent (Cat.1861426 and 22663, Rockford, IL), and ~5 μg of total protein lysate was loaded in each lane. Samples were run on 12% SDS–PAGE, transferred to

PVDF membrane, and blocked for 1 h at room temperature. Membranes were probed with mouse-anti-α-tubulin (4A1; at 1:100; Piperno and Fuller, 1985), mouse-anti-β-tubulin (E7; at 1:100; Developmental Hybridoma Studies Bank, University of Iowa), mouse-anti-c-myc (9E10; at 1:2000; Covance), and rabbit-anti-Zwf1 (Glucose-6-phosphate dehydrogenase; Sigma A9521; at 1:10,000), followed by goat-anti-mouse-680 (LI-COR 926-68070, Superior, NE; at 1:15000) and goat-anti-rabbit-800 (LI-COR 926-32211; at 1:15000) and imaged on an Odyssey Imager (LI-COR Biosciences). Band intensities were quantified using ImageJ.

Solid growth assay
Cells were grown in rich liquid media or selective dropout media for strains carrying a plasmid to saturation at 30°C, and a 10-fold dilution series of each culture was spotted to either rich media plates or rich media plates supplemented with 5 or 10 µg/ml benomyl. Plates were grown at the indicated temperature for the indicated amount of time.

Synchronized cell cycle experiment
Cells were grown overnight in rich liquid media in a shaking incubator at 30°C to early log phase. Cells were pelleted, resuspended in fresh media with 5 µg/ml α-factor, and returned to the shaking incubator at 30°C for 1.5 h, and then an additional 5 µg/ml α-factor was added for an additional 1.5 h at 30°C. Cells were then washed three times with sterile water and resuspended in fresh media with 50 µg/ml *Streptomyces griseus* protease added for synchronous release through START. Wild-type cells were treated with either 1% dimethyl sulfoxide (DMSO) or 5 µg/ml benomyl in DMSO as indicated. The cells were then incubated at 15°C while shaking and fixed at the indicated timepoint as described above. Microtubule labeled with GFP-Tub1 and SPBs labeled with Spc110-tdtomato were imaged as described above.

Cells were segmented using a custom ImageJ macro previously described (Fees *et al.*, 2016). The data were blinded for analysis, and the segmented cells were visually scored for cell cycle stage.

REFERENCES
Abe F (2007). Induction of DAN/TIR yeast cell wall mannoprotein genes in response to high hydrostatic pressure and low temperature. FEBS Lett 581, 4993–4998.

Aguilera J, Randez-Gil F, Prieto JA (2007). Cold response in saccharomyces cerevisiae: New functions for old mechanisms. FEMS Microbiol Rev 31, 327–341.

Aiken J, Buscaglia G, Sophie Aiken A, Moore JK, Bates EA (2019). Tubulin mutations in brain development disorders: Why haploinsufficiency does not explain TUBA1A tubulinopathies. Cytoskeleton 77, 40–54.

Aiken J, Sept D, Costanzo M, Boone C, Cooper JA, Moore JK (2014). Genome-wide analysis reveals novel and discrete functions for tubulin carboxy-terminal tails. Curr Biol 24, 1295–1303.

Alushin GM, Lander GC, Kellogg EH, Zhang R, Baker D, Nogales E (2014). High-resolution microtubule structures reveal the structural transitions in Aβ-Tubulin upon GTP hydrolysis. Cell 157, 1117–1129.

Amberg DC, Burke DJ, Strathern JN (2000). Methods in Yeast Genetics: A Cold Spring Harbor Laboratory Course Manual, 2005 ed., Cold Spring Harbor, NY: Cold Spring Harbor Laboratory.

Berry RW, Shelanski ML (1972). Interactions of tubulin with vinblastine and guanosine triphosphate. J Mol Biol 71, 71–80.

Bhamidipati A, Lewis SA, Cowan NJ (2000). ADP ribosylation factor-like protein 2 (Arl2) regulates the interaction of tubulin-folding cofactor D with native tubulin. J Cell Biol 149, 1087–1096.

Bordas J, Mandelkow E-M, Mandelkow E (1983). Stages of tubulin assembly and disassembly studied by time-resolved synchrotron X-ray scattering. J Mol Biol 164, 89–135.

Borisy GG, Marcum JM, Olmsted JB, Murphy DB, Johnson KA (1975). Purification of tubulin and associated high molecular weight proteins from porcine brain and characterization of microtubule assembly in vitro. Ann NY Acad Sci 253, 107–132.

Breton S, Brown D (1998). Cold-induced microtubule disruption and relocalization membrane proteins in kidney epithelial. J Am Soc Nephrol 9, 155–166.

Breton A, Pinson B, Coulpier F, Giraud MF, Dautant A, Daignan-Fornier B (2008). Lethal accumulation of guanylic nucleotides in saccharomyces cerevisiae HPT1-deregulated mutants. Genetics 178, 815–824.

Carlier MF, Didry D, Pantaloni D (1987). Microtubule elongation and guanosine 5′-triphosphate hydrolysis. role of guanine nucleotides in microtubule dynamics. Biochemistry 26, 4428–4437.

Carlier MF, Pantaloni D (1978). Kinetic analysis of cooperativity in tubulin polymerization in the presence of guanosine Di- or triphosphate nucleotides. Biochemistry 17, 1908–1915.

Carlier MF, Pantaloni D (1981). Kinetic analysis of guanosine 5′-triphosphate hydrolysis associated with tubulin polymerization. Biochemistry 20, 1918–1924.

Correia JJ, Williams RC (1983). Mechanisms of assembly and disassembly of microtubules. Annu Rev Biophys Bioeng 12, 211–235.

Cyert MS, Philpott CC (2013). Regulation of cation balance in saccharomyces cerevisiae. Genetics 193, 677–713.

Fees CP, Aiken J, O'Toole ET, Giddings TH, Moore JK (2016). The negatively charged carboxy-terminal tail of β-tubulin promotes proper chromosome segregation. Mol Biol Cell 27, 1786–1796.

Fees CP, Estrem C, Moore JK (2017). High-resolution imaging and analysis of individual astral microtubule dynamics in budding yeast. J Vis Exp e55610–e55610.

Fees CP, Moore JK (2018). Regulation of microtubule dynamic instability by the carboxy-terminal tail of β-tubulin. Life Sci Alliance 1, e201800054.

Fygenson DK, Braun E, Libchaber A (1994). Phase diagram of microtubules. Physical Review E 50, 1579–1588.

Gao Y, Vainberg I, Chow R, Cowan NJ (1993). Two cofactors and cytoplasmic chaperonin. Mol Cell Biol 13, 2478–2485.

Gell C, Bormuth V, Brouhard GJ, Cohen DN, Diez S, Friel CT, Helenius J, Nitzsche B, Petzold H, Ribbe J, et al. 2010. Microtubule dynamics reconstituted in vitro and imaged by single-molecule fluorescence microscopy. Vol. 95.

Geyer EA, Burns A, Lalonde BA, Ye X, Piedra F-A, Huffaker TC, Rice LM (2015). A mutation uncouples the tubulin conformational and GTPase cycles, revealing allosteric control of microtubule dynamics. ELife 4, e10113.

Gladfelter AS, James TY, Amend AS (2019). Marine fungi. Curr Biol 29, R191–R195.

Gupta ML, Bode CJ, Dougherty CA, Marquez RT, Himes RH (2001). Mutagenesis of β-tubulin cysteine residues in saccharomyces cerevisiae: Mutation of cysteine 354 results in cold-stable microtubules. Cell Motil Cytoskeleton 49, 67–77.

Gupta ML, Bode CJ, Thrower D, Pearson CG, Suprenant KA, Bloom KS, Himes RH (2002). β-tubulin C354 mutations that severely decrease microtubule dynamics do not prevent nuclear migration in yeast. Mol Biol Cell 13, 2919–2932.

Halachmi D, Eilam Y (1989). Cytosolic and vacuolar Ca2+ concentrations in yeast measured with Ca2+ sensitive dye indol 1. FEBS Lett 256, 55–61.

Hamel E, Batra JK, Huang AB, Lin CM (1986). Effects of PH on tubulin-nucleotide interactions. Arch Biochem Biophys 245, 316–330.

Himes RH, Detrich HW (1989). Dynamics of antarctic fish microtubules at low temperatures. Biochemistry 28, 5089–5095.

Howes SC, Geyer EA, LaFrance B, Zhang R, Kellogg EH, Westermann S, Rice LM, Nogales E (2017). Structural differences between yeast and mammalian microtubules revealed by Cryo-EM. J Cell Biol 216, 2669–2677.

Huff LM, Sackett DL, Poruchynsky MS, Fojo T (2010). Microtubule-disrupting chemotherapeutics result in enhanced proteasome-mediated degradation and disappearance of tubulin in neural cells. Cancer Res 70, 5870–5879.

Hyman AA, Chretien D, Arnal I, Wade RH (1995). Structural changes accompanying GTP hydrolysis in microtubules: Information from a slowly

hydrolyzable analogue guanylyl-(alpha,beta)-methylene- diphosphonate. J Cell Biol 128, 117–125.

Inoué S (2010). Effect of temperature on the birefringence of the mitotic spindle. In: Collected Works of Shinya Inoué. Singapore: WORLD SCIENTIFIC, 109–110.

Jordan MA, Toso RJ, Thrower D, Wilson L (1993). Mechanism of mitotic block and inhibition of cell proliferation by taxol at low concentrations (HeLa cells/microtubule dynamics/vinblastine). Proc Natl Acad Sci USA 90, 9552–9556.

Kortazar D, Fanarraga ML, Carranza G, Bellido J, Villegas JC, Avila J, Zabala JC (2007). Role of cofactors B (TBCB) and E (TBCE) in tubulin heterodimer dissociation. Exp Cell Res 313, 425–436.

Kováč L (1985). Calcium and *Saccharomyces cerevisiae*. Biochim Biophys Acta – General Subjects 840, 317–323.

Lacefield, S and Solomon, F (2003). A novel step in β-tubulin folding is important for heterodimer formation in saccharomyces cerevisiae. Genetics 165, 531–541.

Lange G, Mandelkow EMM, Jagla A, Mandelkow E (1988). Tubulin oligomers and microtubule oscillations: Antagonistic role of microtubule stabilizers and destabilizers. Eur J Biochem 178, 61–69.

Lee JC, Timasheff SN (1977). In vitro reconstitution of calf brain microtubules: Effects of solution variables. Biochemistry 16, 1754–1764.

Libkind D, Hittinger CT, Valério E, Gonçalves C, Dover J, Johnston M, Gonçalves P, Sampaio JP (2011). Microbe domestication and the identification of the wild genetic stock of lager-brewing yeast. Proc Natl Acad Sci USA 108, 14539–14544.

Lin MC, Galletta BJ, Sept D, Cooper JA (2010). Overlapping and distinct functions for cofilin, coronin and Aip1 in actin dynamics in vivo. J Cell Sci 123, 1329–1342.

Mandelkow EM, Mandelkow E, Milligan RA (1991). Microtubule dynamics and microtubule caps: A time-resolved cryo-electron microscopy study. J Cell Biol 114, 977–991.

Manka SW, Moores CA (2018). The role of tubulin–tubulin lattice contacts in the mechanism of microtubule dynamic instability. Nat Struct Mol Biol 25, 607–615.

McIntosh JR, O'Toole E, Morgan G, Austin J, Ulyanov E, Ataullakhanov F, Gudimchuk N (2018). Microtubules grow by the addition of bent guanosine triphosphate tubulin to the tips of curved protofilaments. J Cell Biol 217, 2691–2708.

Mitchison T, Kirschner M (1984). Dynamic instability of microtubule growth. Nature 312, 237–242.

Nithianantham S, Le S, Seto E, Jia W, Leary J, Corbett KD, Moore JK, Al-Bassam J (2015). Tubulin cofactors and Arl2 are cage-like chaperones that regulate the soluble Aβ-tubulin pool for microtubule dynamics. ELife 4, DOI:10.7554/eLife.08811.

Olmsted JB, Borisy GG (1973). Microtubules. Annu Rev Biochem 42, 507–540.

Olmsted JB, Marcum JM, Johnson KA, Allen C, Borisy GG (1974). Microtubule assembly: Some possible regulatory mechanisms. J Supramol Struct 2, 429–450.

Ou J, Ball JM, Luan Y, Zhao T, Miyagishima KJ, Xu Y, Zhou H, Chen J, Merriman DK, Xie Z, et al. (2018). IPSCs from a hibernator provide a platform for studying cold adaptation and its potential medical applications. Cell 173, 851–863.e16.

Petracek ME, Longtine MS (2002). PCR-based engineering of yeast genome. Methods Enzymol 350, 445–469.

Piperno G, Fuller MT (1985). Monoclonal antibodies specific for an acetylated form of α-tubulin recognize the antigen in cilia and flagella from a variety of organisms. J Cell Biol 101, 2085–2094.

Purich DL, Kristofferson D (1984). Microtubule assembly: A review of progress, principles, and perspectives. Adv Protein Chem 36, 133–212.

Romani A, Scarpa A (1992). Regulation of cell magnesium. Arch Biochem Biophys 298, 1–12.

Serna M, Carranza G, Martín-Benito J, Janowski R, Canals A, Coll M, Zabala JC, Valpuesta JM (2015). The structure of the complex between α-Tubulin, TBCE and TBCB reveals a tubulin dimer dissociation mechanism. J Cell Sci 128, 1824–1834.

Sheff MA, Thorn KS (2004). Optimized cassettes for fluorescent protein tagging in saccharomyces cerevisiae. Yeast 21, 661–670.

Sikorski RS, Hieter P (1989). A system of shuttle vectors and yeast host strains designed for efficient manipulation of DNA in saccharomyces cerevisiae. Genetics 122, 19–27.

Sobel SG, Snyder M (1995). A highly divergent γ-tubulin gene is essential for cell growth and proper microtubule organization in saccharomyces cerevisiae. J Cell Biol 131, 1775–1788.

Song S, Lee KS (2001). A novel function of saccharomyces cerevisiae CDC5 in cytokinesis. J Cell Biol 153, 451–469.

Spiegelman BM, Penningroth SM, Kirschner MW (1977). Turnover of tubulin and the N Site GTP in chinese hamster ovary cells. Cell 12, 587–600.

Tian G, Bhamidipati A, Cowan NJ, Lewis SA (1999). Tubulin folding cofactors as GTPase-activating proteins. GTP hydrolysis and the assembly of the α/β-tubulin heterodimer. J Biol Chem 274, 24054–24058.

Tian G, Cowan NJ (2013). Tubulin-specific chaperones: Components of a molecular machine that assembles the α/β heterodimer. Methods Cell Biol 115, 155–171.

Tian G, Huang Yi, Rommelaere H, Vandekerckhove J, Ampe C, Cowan NJ (1996). Pathway leading to correctly folded β-tubulin. Cell 86, 287–296.

Tian G, Kong XP, Jaglin XH, Chelly J, Keays D, Cowan NJ (2008). A pachygyria-causing α-tubulin mutation results in inefficient cycling with CCT and a deficient interaction with TBCB. Mol Biol Cell 19, 1152–1161.

Tian G, Lewis SA, Feierbach B, Stearns T, Rommelaere H, Ampe C, Cowan NJ (1997). Tubulin subunits exist in an activated conformational state generated and maintained by protein cofactors. J Cell Biol 138, 821–832.

Tilney LG, Porter KR (1967). Studies on the microtubules in heliozoa. II. The effect of low temperature on these structures in the formation and maintenance of the axopodia. J Cell Biol 34, 327–343.

Vainberg IE, Lewis SA, Rommelaere H, Ampe C, Vandekerckhove J, Klein HL, Cowan NJ (1998). Prefoldin, a chaperone that delivers unfolded proteins to cytosolic chaperonin. Cell 93, 863–873.

Walker RA, O'Brien ET, Pryer NK, Soboeiro MF, Voter WA, Erickson HP, Salmon ED (1988). Dynamic instability of individual microtubules analyzed by video light microscopy: Rate constants and transition frequencies. J Cell Biol 107, 1437–1448.

Weber K, Pollack R, Bibring T (1975). Antibody against tuberlin: The specific visualization of cytoplasmic microtubules in tissue culture cells. Proc Natl Acad Sci USA 72, 459–463.

Weisenberg RC (1972). Microtubule Formation in vitro in solutions containing low calcium concentrations. Science 177, 1104–1105.

Weisenberg RC, Borisy GG, Taylor, EW (1968). The colchicine-binding protein of mammalian brain and its relation to microtubules. Biochemistry 7, 4466–4479.

Yaffe MB, Farr GW, Miklos D, Horwich AL, Sternlicht ML, Sternlicht H (1992). TCP1 complex is a molecular chaperone in tubulin biogenesis. Nature 358, 245–248.

Zhang R, Alushin GM, Brown A, Nogales E (2015). Mechanistic origin of microtubule dynamic instability and its modulation by EB proteins. Cell 162, 849–859.

Zheng Y, Wong ML, Alberts B, Mitchison T (1995). Nucleation of microtubule assembly by a γ-tubulin-containing ring complex. Nature 378, 578–583.